A New Two-Impinging-Streams Heterogeneous Reactor

KFIR LUZZATTO,
ABRAHAM TAMIR
AND ISAAK ELPERIN

Department of Chemical Engineering
Ben Gurion University of the Negev
Beer Sheva, Israel

The characteristics of a new heterogeneous reactor of the "two impinging streams" type, suitable for gas-solid heat and mass-transfer operations, were investigated.

The operating limits of the reactor, with respect to gas and solid particles mass flow rate and pressure drop, were determined; scale-up criteria with respect to the hydrodynamics of the reactor were also established. It has been found that, under certain conditions, the introduction of solid particles into the gas stream lowers the pressure drop on the reactor. In addition, the maximal pumping energy per kg of solids transported through the reactor by the air is much lower than in a fluidized-bed-type reactor.

A stochastic model based on Markov processes was developed which closely describes the behavior of the solid particles in the reactor. A technique based on this model was employed for determining the residence time distribution of the particles in the reactor.

SCOPE

The fluidized-bed reactors, which are widely employed in the chemical industry to carry out heat and mass transfer operations between solid particles and a gaseous phase, present the considerable drawback of being limited to low relative velocities between the solid particles and the surrounding gas because of solids carryover. Consequently, the maximal obtainable heat and mass-transfer rates, which are proportional to the said relative velocity, are limited.

The new two-impinging-streams reactor overcomes this limitation through an entirely different flow behavior which incorporates countercurrent flow of two identical streams of particles carrying gas. As a result, oscillatory motion of the solid particles is created and high relative velocities are obtained. Gas flow velocities in the order of 50 m/s may be reached in this reactor, in comparison to 1-3 m/s usually obtained in fluidized-bed reactors.

The objective of the present work is to obtain basic information on the performance of the reactor. This comprises: pressure drop measurements in the presence and in the absence of solid flowing particles; data on the maximal permissible mass flow rates of gas phase (air) and solid particles; and residence time distribution of the solid particles. Further, it provides a theoretical model which describes the behavior and the flow paths of the solid particles in the reactor which can help gain some insight of the phenomena occurring therein.

Since the nature of the dispersion of solid particles in air is highly noncontinuous under the conditions which we desired to investigate, a new technique was developed to obtain correct residence time distribution curves from the response of the reactor to a pulse input signal. The technique incorporates a theoretical model which is based on Markov stochastic processes.

CONCLUSIONS AND SIGNIFICANCE

Pressure drop measurements were carried out in the presence of solid particles having a mean diameter of 1.9×10^{-3}m and with air alone to characterize the power requirements of the investigated reactor. The measurements showed that the pumping work per kg of particles fed to the reactor is significantly lower than in a fluidized-bed reactor. The graph of the *Eu* number vs. the *Re* number is continuously decreasing until it reaches a constant value. In this region, scale-up using the curves of Figure 2a requires only geometrical similitude because the effect of the hydrodynamic conditions is negligible. In the range in which *Eu* varies as a function of *Re*, the scale-up requires both geometrical and hydrodynamic similitudes. Plotting the ratio of the Euler number obtained with flowing particles to the one resulting from the flow of air alone, vs. the ratio of the mass flow rate of the particles to that of air alone, yields a straight line.

Operating limits for the mass flow rates of air and solid particles and the chocking point of the reactor were determined. It was observed that, at high Reynolds numbers, the pressure drop on the reactor decreased when solid particles were introduced into a stream of particles-free air. This result is suggestive of the reduction of strong vortex motion of the air by the presence of solid particles in the flowing stream.

A stochastic model of the behavior of solid particles flowing through the reactor was developed and successfully tested. The model was then employed to help determine proper residence time distribution (RTD) curves. The RTD was experimentally determined by means of a very simple device which was developed for this purpose.

Direct observation of the motion of the particles within the reactor indicated that they exhibit a strong oscillatory behavior. This was also confirmed by the fact that, by increasing the air flow rate, the mean residence time of the particles flowing through the reactor is increased.

The results herein reported lie the basis for extensive theoretical and applied research on the various aspects and applications of this new reactor.

Correspondence concerning this paper should be addressed to A. Tamir.

INTRODUCTION

One of the most important operations in chemical engineering and other fields of technology is the mass or heat transfer between solid particles and a gaseous phase. This operation is usually carried out in fixed- or fluidized-bed reactors which gained wide attention from the point of view of both theoretical and applied research (Leva, 1959; Kunii and Levenspiel, 1969). Notwithstanding its many advantages, the fluidized-bed reactor presents a considerable drawback that the relative velocity between the solid particles and the surrounding gas phase is relatively low, about 1 to 3 m/s, owing to solids carryover. Consequently, since the heat and mass transfer rates are linearly proportional to the relative velocity, the transport phenomena occurring within the reactor are accordingly limited.

This drawback has been accepted as unavoidable for a long time; however, the following analysis will show how both the absolute gas velocity $\tilde{U}_a$ and the solid-gas relative velocity U can be appreciably increased. Assume that two streams of solids-carrying gas flow against each other in a countercurrent flow. Assume that the relative velocity between the particles and the gas phase in each stream to be zero, and the gas velocity of each stream $\tilde{U}_a$. Then, at the zone in which the two streams impinge the relative velocity U between the particles in one stream and the gas in the second stream is:

$$U = \tilde{U}_a - (-\tilde{U}_a) = 2\tilde{U}_a \qquad (1)$$

The above relation reveals that the relative velocity can reach twice the absolute velocity $\tilde{U}_a$. The latter can be significantly increased by means of countercurrent flow of two streams of solids-carrying gas. Furthermore, in countercurrent operations it is possible to accomplish, under certain operating conditions, a harmonic motion of the particles which will increase the residence time thereof in the zone of high relative velocities. It is obvious that, by increasing at the same time the relative velocity and the residence time, the transort phenomena are enhanced and the size of the equipment required for a certain operation will be probably significantly smaller than that of a fluidized-bed reactor.

Elperin and Tamir (Patent, 1982), Elperin et al. (1982), and Tamir et al. (1983) demonstrated the realization of the above concepts by means of a new two-impinging-streams heterogenous reactor with oscillatory motion of solid particles. Preliminary experimental work showed a high efficiency in evaporation operations and that this reactor can be employed as a multipurpose tool for carrying out various heat and mass transfer operations.

A stochastic model was established which enables us to predict the behavior of the reactor. In addition, the hydrodynamics of the reactor was investigated and a new method was developed for obtaining residence time distribution curves of the solid particles, which incorporates the stochastic model for the interpretation of the experimental data.

REACTOR

The reactor comprises the following elements, Figure 1:

a) Two gas-feeding pipes 2.

b) Particles screw—feeder 3.

c) Inlet 4 of gas and dispersed particles to the reactor.

d) Annular space 1 (between points 9 and 11) in which intensive contact between gas phase and solid particles takes place; the so-called "reaction-zone."

e) Separation zone, for air particles separation, located between points 10 and 11 in the annular space 1.

f) Swirling blades 6, which cause the particles to move radially towards the walls of the reactor and hence to be discharged through opening 8.

g) Conical section 7 and reactor outlet 8 for particles discharge.

h) Gas outlet pipe 5.

i) Pressure tap 13 for measuring the pressure drop between the reactor inlet and the gas outlet 5.

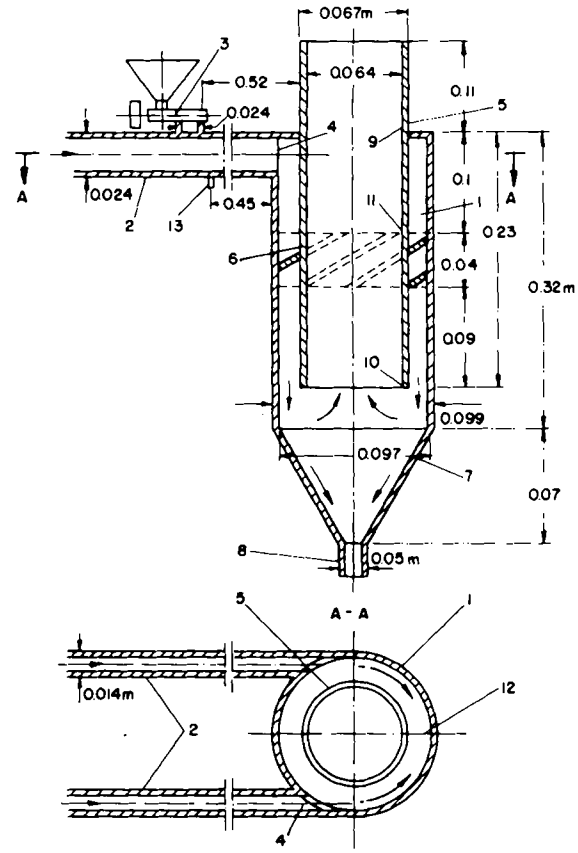

Figure 1. Multipurpose single-stage heterogeneous reactor.

The reactor operates as follows. Gas is fed by means of an appropriate blower through two identical pipes 2, symmetrically positioned with respect to the annular upper portion of the reactor. The solid particles are fed at a constant mass flow rate to the gas stream by means of a screw feeder 3, placed some 0.5 m before the entrance to the reactor. This enables the solid particles to accelerate to some extent before entering the reactor at point 4, thus preventing them from falling downwards and be immediately discharged. The location of the particles feed point is clearly dictated by their size and density. The two gas streams which carry the solid particles tangentially enter the annular space 1. The gas-particles streams impinge at point 12, symmetrically positioned with respect to the entrance points 4 of the streams. Two particles in the two countercurrent streams may exhibit the following behaviors: they may experience direct collision as a result of which they fall immediately downwards. In case that direct collision does not occur or that they only slightly touch one another, the particles penetrate from one gas stream into the other, first lose their velocity and then are accelerated by the other stream in a direction opposite to their original one. This causes a harmonic motion of the particles along the perimeter of the annular contact zone 1, while their velocity and direction change according to their position with respect to the impingement point. It is readily understood that the harmonic motion accomplished in the reaction zone permits to achieve very high slip velocities (Eq. 1). After several oscillations, the particles loose their speed due to collisions among themselves as well as with the walls of the reactor, and are carried away from the active zone 1 by the gas stream flowing out. The particles-gas stream then reaches the separation zone located between points 10 and 11 in Figure 1, and meets, first the swirling blades 6 which impose on the particles a centrifugal force in the direction of the reactor walls and hence they are discharged through opening 8 of the conical section 7. The particles-free gas flows upwards through the inner pipe 5, like in a cyclon. The upper part of the reactor, through which pipe 5 was inserted, was made from transparent plastic which made it possible to observe the particles' behavior at the

TABLE 1. RANGE OF OPERATING CONDITIONS OF THE REACTOR

	Minimal	Maximal
Air Mass Flow Rate, w_a (kg/s)	0.001	0.013
Particles Mass Flow Rate, w_p (kg/s)	0	0.039
Air Velocity in Inlet Pipes to Reactor, U_a (m/s)	1.7	20
Pressure Drop in the Reactor without Particles Flow, ΔP_a (Pa)	9.8	1127
As Above, with Particles Flow, ΔP_p (Pa)	19.6	2255
Mean Residence Time, τ(s)	1	4
Euler Number for Air Flow Only, Eu_a	0.43	0.58
Euler Number with Particles Flow Eu_p	0.40	0.89
Inlet Pipe Hydraulic Diameter, D(2 in Figure 1, m)	—	0.018
Specific Pumping Energy, kJ/kg Particles	—	0.47
Particles Mean Diameter, D_p (m)	—	1.9×10^{-3}
Particles True Density, kg/m^3	—	1158
Particles Bulk Density, kg/m^3	—	730
Number of Particles per Gram	—	206

impingement zone. It should be noted that Figure 1 describes a single-stage reactor. However, several such reactors can easily be assembled to be operated as a multistage reactor, as described by Elperin and Tamir (Patent, 1982). The range of the operating conditions of the reactor is given in Table 1 (Patent, 1982).

HYDRODYNAMICS

To test the hydrodynamic behavior of the reactor, pressure drop measurements were carried out between the reactor inlet and the air outlet which corresponds to atmospheric pressure (points 13 and 9 in Figure 1). The measurements were made at different Reynolds number and solid particles mass flow rates. The particles employed for these tests were vegetable grains (millet seeds) having a mean diameter $D_p = 1.9 \times 10^{-3}$m and density $\rho_p = 1{,}153$ kg/m^3.

The results of three tests, in terms of Euler numbers, are shown in Figure 2a as a function of a Reynolds number based on the inlet pipes diameter. The above quantities are defined a follows:

$$Eu = \frac{\Delta P}{\rho_a U_a^2} \tag{2}$$

$$Re = \frac{DU_a}{\nu_a} \tag{3}$$

where in general Eu vs. Re is a function of the particles diameter, density, shape and mass flow rate.

Inspection of the curves in Figure 2a revealed the following characteristic behavior:

a) at a Reynolds number of about 11,000–13,000, the lines representing the experiments carried out in the presence of flowing particles cut the curve describing the flow of air alone. Thus, lower energy expenditures are involved while operating at high Reynolds numbers (and consequently at high slip velocities). This behavior may be explained as follows. By increasing the gas velocity in the absence of particles flow, turbulence in the gas stream is enhanced with possible formation of vortex motion. The introduction of solid particles into the flowing gas causes part of the energy to be converted into kinetic energy of the particles rather than into expansive turbulence. Consequently, at high gas flow rates, the pressure drop in the presence of particles flow might be lower than in the absence of solid flowing particles.

b) At high Reynolds numbers the curves in Figure 2 become parallel to the Re axis; the Eu number is independent of the hydrodynamic conditions. The curves of Figure 2a are useful for scale-up purposes. In the region of constant Eu, the prediction of working conditions from laboratory-scale experiments requires to maintain geometrical similitude between the laboratory apparatus and the large-scale equipment (Gukhman, 1973; Mikheev and Mikheeva, 1977). In other words it is necessary that:

$$\overline{Eu} = 1 \text{ and } \overline{L} = 1 \tag{4-1}$$

In the region where the Eu number varies as a function of the Re number, the following conditions must hold for scale-up:

$$\overline{Eu} = 1, \quad \overline{L} = 1 \text{ and } \overline{Re} = 1 \tag{4-2}$$

To set useful operating limits for the reactor it was essential to investigate the response of the system to different concentrations of solid particles in the inflowing gas stream. For this purpose chocking tests have been carried out in which at a constant particles mass flow rate, the air flow rate was continuously decreased until, at a certain point, the pressure drop increased very rapidly and the reactor chocked. Figure 2b demonstrates this behavior and presents all the curves of Figure 2a by means of generalized curve and dimensionless variables.

The ratio:

$$\eta = Eu_p/Eu_a \tag{5}$$

In Figure 2b, of the Euler number in the presence of solid particles divided by the Euler number in the absence of solid particles flow at the same Reynolds number, is plotted vs.

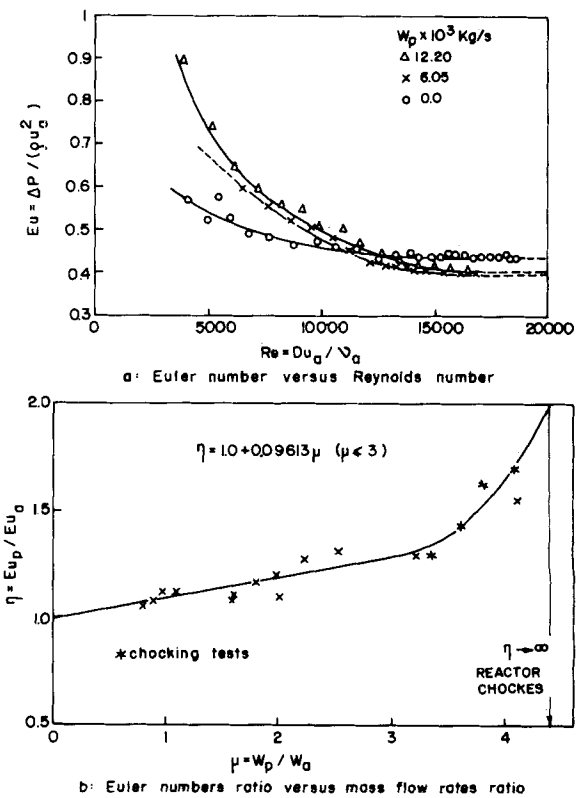

Figure 2. Hydrodynamics of a two-impinging-streams reactor.

$$\mu = w_p/w_a \tag{6}$$

which is the ratio of the mass flow rate of the particles to that of air alone. It has been found that, at a value of about $\mu = 4.4$, η goes to infinity and the reactor chockes. The recommended maximal value of μ, however, should not exceed the value of 3. The experimental relation which has been found to hold, up to $\mu = 3$, is:

$$\eta = 1.0 + 0.09613\mu \tag{7}$$

The curve of Figure 2b has two useful applications:

1. When such a plot is obtained for a given reactor, for which the Eu_a dependency is known, Figure 2b can be used to evaluate Eu_p, for any desired ratio μ.
2. The same can be done for any other different reactor, using a plot previously obtained for a laboratory-scale reactor, provided that geometrical similitude is maintained, and that the reactor is operated in the zone of constant Eu.

Thus, we are able to perform the optimization of a projected reactor, based on equipment size and feed mass flow rates ratio, either by means of Figure 2b or of Eq.7.

RESIDENCE TIME DISTRIBUTION

Determination of RTD

The determination of the RTD of the solid particles in this reactor is important because of the oscillatory motion of the particles at the impingement zone, which might cause internal recirculation with throughflow and affect the mean residence-time. The determination of the RTD presents many difficulties and problems for the following reasons:

1. The number of particles flowing through the reactor is very low, 10^3 particles/s for typical mass flow rate of 5×10^{-3} kg/s, in comparison to 10^6 particles/s should sand be used. Consequently, only a small number of tagged particles can be used in tracer experiments without affecting the flow conditions. In our RTD experiments about 200 tracer particles were used in comparison to 2×10^5 particles in the case of sand.
2. The mean residence time of the system lies in the range of τ = 1–4 seconds. Therefore, the tracer must be injected into the system during very short injection times to approach a true dirac function and obtain useful results.

The choice of the tracer detection technique at the reactor exit was influenced by the aforesaid factors.

A continuous radioactive technique, detecting radioactively tagged particles at the exit of the reactor (or elsewhere), would reveal the behavior schematically shown in Figure 3(a), for the case of 200 particles of tracer. Each curve corresponds to a single pulse experiment in which the number of particles (i.e., number of countings) is recorded as a function of time and only three curves are shown out of m experiments, each carried out under identical operation conditions. It is clearly seen that m-different curves can be obtained for m-identical experiments. Furthermore, at certain times the radioactive detector may indicate total absence of tagged particles at the detecting position. Such phenomena are typical of situations where the number of the counted particles is very small; that is, the behavior of the investigated phase is highly noncontinuous with respect to the length of the observed phenomenon. Under such conditions, the random fluctuations of the single particles become detectable and a reproduction of the results obtained in the experiments is impossible, Figure 3(a). An "average" behavior, which is of practical use, is that shown in Figure 3(b) in which the mean concentration $\bar{C}$ at a certain t is calculated according to the formula:

$$\bar{C} = \frac{\sum_{i=1}^{m} C_i}{m} \tag{8}$$

C_i, which is the number of tagged particles (or concentration) corresponding to a specific experiment i, is obtained from the values of Figure 3(a) for a certain t. m is the number of repetitive experiments which are carried out until no significant change is observed in the behavior of Figure 3(b).

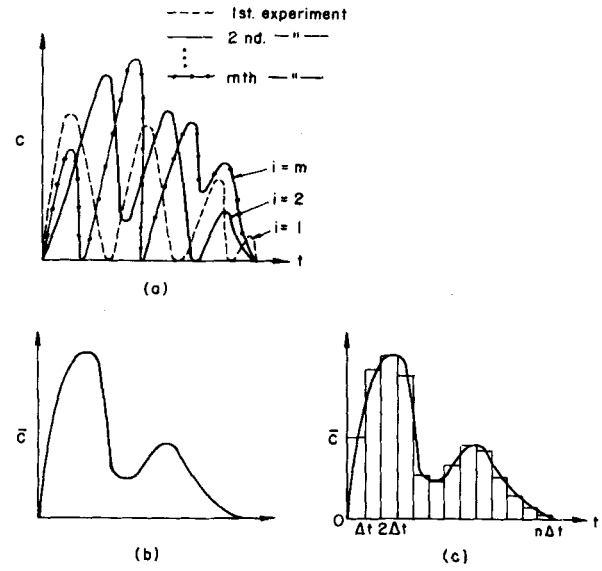

Figure 3. System response to a pulse input in a noncontinuous particles system.

As it is easily understood, obtaining the required curve of Figure 3(b) involves repetitive experiments and statistical averaging, all of which require a considerable amount of work and time. However, there is a simpler and easier way to obtain the desired curve, Figure 3(c). Assume that we take, instead of instantaneous readings, cumulative (viz., mixed-cup) readings of the response for each experiment, each reading being collected during an interval of time Δt. It is clear that, as we increase the length of the sampling interval Δt from zero (which corresponds to instantaneous reading) to the value Δt of Figure 3(c), we decrease the sensitivity of our readings until, at a certain value, the random fluctuations of the particles are not felt any more. At this value of Δt, all the m curves of Figure 3(a) will yield the same result and a single experiment will suffice to obtain the curve of Figure 3(c), which is identical to that obtained by Eq. 8. The problem which remains is to determine which value of Δt to employ in each experiment, since Δt must be large enough so that random oscillations are eliminated, but not so large that useful information is lost.

As a result of the above facts, the device shown in Figure 4(d) has been developed, which comprises a circular plate divided in several equal sections. The plate is placed under the solid discharge opening of the reactor as shown in Figure 4(e), and is rotated by means of an electrical motor. Different sampling intervals can be obtained by changing the speed of rotation and the number of divisions of the plate (i.e., the time needed for a triangular section to pass under the solid particles discharge opening). Special care has been taken to choose angular velocities such that in any case the last 3–4 sections of the rotating plate will be free of tagged particles, thereby assuring that all the tracer has been collected during the experiment. Pulse experiments have been carried out to determine the RTD. For this purpose, two identical syringes have been positioned as close as possible to the particles inlet, before point 3 of Figure 1. The two syringes were charged with colored particles easily recognizable from the main stream particles.

The concentration of the tagged particles at different time intervals is obtained by separating and counting the coloured particles found in each section of the device of Figure 4(d,e). The syringes were actuated together by a common lever which, when pushed downwards by pneumatic means, releases the tagged particles into the stream of gas. Injection time of 0.08 seconds has been measured with syringes containing about 100 particles each. This has been done by filming the downwards motion of the lever and, at the same time, an electronic stop-watch, by means of a high-speed camera.

However, while operating with this experimental setup, different $\overline{C}$ curves were obtained by varying the speed of rotation of the circular plate. This, of course, was caused by the small number of tagged particles which it was possible to employ, under the desired operation conditions. Thus the problem was how to obtain a true RTD curve, where by "true curve" it is meant a curve obtained from a representative population of particles in which random oscillations due to the "personal" behavior of the single particle are not felt any more, as previously discussed with reference to Figure 3.

It is common knowledge that there is a maximal length of time interval for sampling the response of a system to a certain input signal. When measuring quantities related to continuous media, however, any time interval shorter than the maximum will provide a better resolution and will therefore be highly desirable. Furthermore, in continuous systems (like water or gases) it is possible to reach a sampling speed that, even if considerably increased, will not produce any detectable change in the response curve. In addition, in such systems only a small sample of the exiting stream needs be tested because of the homogeneity of properties obtained in liquids or gases and there is no need to perform the response measurements on the whole material stream. Unfortunately, this is not the case in systems of dispersed particles like ours. Therefore, if sampling time intervals are chosen which are too short, the experimental shift from the true values increases rapidly, leading to incorrect measured values. However, a sampling time interval which is too large will also produce unsatisfactory results.

The true curve has been found by applying a stochastic model developed for the reactor which is based on the discrete Markov processes. The model has been successfully tested and proved a useful tool in obtaining the true RTD curve. The model, which is based on the observed flow paths of the particles within the reactor, also provides some insight into the nature of the phenomena which take place therein.

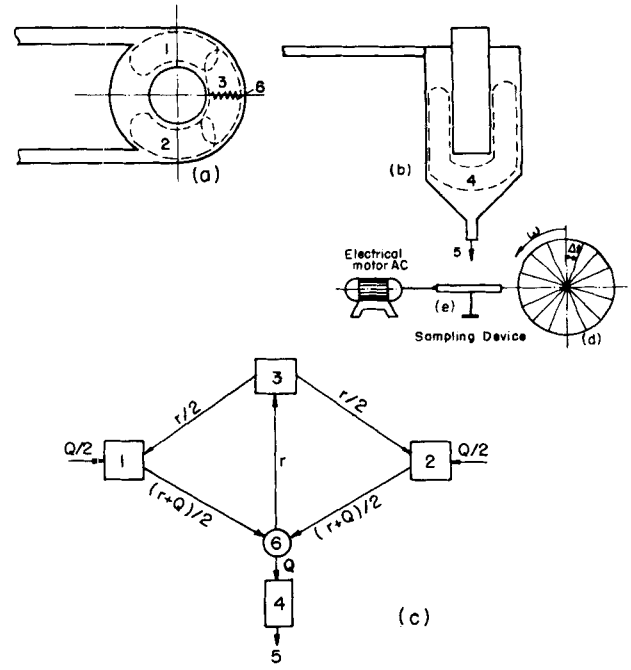

Figure 4. Model of the reactor.

Markov Processes

We limit ourselves here to the definitions and equations related to the discrete Markov process, which are required for the modelling of the reactor. An extensive discussion of Markov processes can be found elsewhere (Howard, 1960).

We define:

p_{ij} = probability of transition of the system from state i to j. In the present case, the system is one particle moving through the reactor. These probabilities are related to the geometry of the reactor and are time-independent

P = transition matrix composed of all possible p_{ij}'s (Eq. 19)

$s_i(n)$ = state probability, the probability of the system to occupy state i after n transitions. These probabilities are time-dependent

$S(n)$ = state probability vector;
$S(n) = [s_1(n), s_2(n), \ldots, s_N(n)]$ (9)

N = number of possible states for transition of the system

$S(0)$ = initial state probability vector

The equations which govern the discrete Markov process are:

$$\sum_{i=1}^{N} s_i(n) = 1 \tag{10}$$

Equation 10 states that the total probability of the system to reach one of all the possible N states which can be occupied after n transitions is equal to unity.

$$s_j(n+1) = \sum_{i=1}^{N} s_i(n) p_{ij}; \quad n = 0,1,2 \ldots \tag{11}$$

which implies that the probability of the system to be in state j after $n+1$ transitions is equal to the sum of its probabilities to be in any state i after n transitions, multiplied by the probability of going from state i to state j in one transition step. This is also true for all the states as expressed by:

$$S(n+1) = S(n) \cdot P \tag{12}$$

Thus, if the state probability vector is known at some time, say at the beginning of the process, Eqs. 11 or 12 enable us to compute, step by step, the probability of the system to be in any one of states i after n transitions ($n = 0,1,2, \ldots$).

The Model of Reactor

The model is of the kind first introduced by Van de Vusse (1962). A model of this type for a stirred vessel has been solved by Gibilaro et al. (1967) by means of a Markov process. However, the situation in the stirred vessel is quite different because of the continuous nature of the medium involved and therefore a discrete Markov process was employed by the above authors to approximate a continuous process.

With reference to Figure 4, the following considerations and assumptions have been done in performing the modelling:

1. There are three main zones in which mixing of particles takes place: zones 1, 2 and 3 in Figure 4(a). These three zones are considered to behave like perfectly mixed vessels.
2. The lower part of the reactor, Figure 4(b), behaves like a plug flow reactor in which no backmixing takes place.
3. The time needed for a particle physically to pass from one vessel to the other is equal to zero. This is true since the actual boarders of one vessel overlap with the neighboring ones. On the other hand, a particle might stay in one of the above zones during a finite period of time.
4. The holdup, v, is equal for each vessel i.

The resulting model is shown in Figure 4(c). It is clear that each vessel represents a "state" in the Markov process and that the transition probability p_{ij} is the probability of a particle to leave vessel i and enter vessel j. It is also reasonable to assume in the present case a recycle stream, designated by r, due to the countercurrent flow. The recycle stream r represents the stream of particles held in zone 1 of the reactor of Figure 1 by harmonic motion, while the impingement line 6 of Figure 4(a) is represented as a circle in Figure 4(c), outside vessel 3, for the sake of clarity.

Let's now look at vessel 4 in Figure 4(b). Whenever a particle reaches this vessel, it leaves the system to state 5 where it remains. State 5 is then a "trapping state." Thus the value of $s_4(n)$ indicates the probability that a particle entering the system at $n = 0$ will leave it after $n\Delta t (n = 1,2, \ldots)$. The knowledge of the numerical

value of $s_4(n)$ for $n = 0,1,2\ldots$ represents the impulse response of the system after n intervals of time length Δt. By rotating the sampling plate device of Figure 5 we obtain a "picture" of the situation within vessel 4 for any Δt, the magnitude of Δt being determined by the rotation speed and the length of the base of each triangular section of the plate. Similarly, the value of $s_5(n)$ represents the response of the system to a unit step, since 5 is an absorbing state and $s_5(n)$ are the cumulative probabilities of the tagged molecules leaving the system after time intervals $\Delta t, 2\Delta t \ldots, n\Delta t$. This is equivalent to adding the values found from the triangular sections of the sampling plate to one another.

It is possible to apply appropriate equations for the various probabilities along the path of a particle form the inlet of the reactor up to the exit.

The probability of a particle to remain in vessel 1, 2 or 3 during a time interval Δt is as follows:

$$p_{11} = p_{22} = e^{-1/2(r+Q)\Delta t/v} \tag{13}$$

$$p_{33} = e^{(-r/v)\Delta t} \tag{14}$$

while the probability of leaving any vessel i is:

$$1 - p_{ij} \tag{15}$$

Q is the particles mass flow rate, v is the holdup of a "vessel" and r is the internal recirculation flow rate.

Thus, the probabilities of a particle to pass from vessel 1 to vessel 3, from vessel 3 to vessel 2 or from vessel 1 to vessel 4 (in Figure 4(c)) are:

$$p_{13} = p_{23} = \frac{r}{r+Q}(1 - e^{-1/2(r+Q)\Delta t/v}) \tag{16}$$

$$p_{32} = p_{31} = 1/2(1 - e^{(-r/v)\Delta t}) \tag{17}$$

$$p_{14} = p_{24} = \frac{Q}{r+Q}(1 - e^{-1/2(r+Q)\Delta t/v}) \tag{18}$$

respectively.

We can now write the complete transition probabilities matrix, as follows:

$$p = \begin{vmatrix} p_{11} & p_{12}\cdots & p_{15} \\ p_{21} & p_{22}\cdots & p_{25} \\ \cdot & \cdot & \cdot \\ \cdot & \cdot & \cdot \\ \cdot & \cdot & \cdot \\ p_{51} & p_{52}\cdots & p_{55} \end{vmatrix}$$

$$= \begin{vmatrix} e^{-1/2(r+Q)\Delta t/v} & 0 & \frac{r}{r+Q}(1 - e^{-1/2(r+Q)\Delta t/v}) & \frac{Q}{r+Q}(1 - e^{-1/2(r+Q)\Delta t/v}) & 0 \\ 0 & e^{-1/2(r+Q)\Delta t/v} & \frac{r}{r+Q}(1 - e^{-1/2(r+Q)\Delta t/v}) & \frac{Q}{r+Q}(1 - e^{-1/2(r+Q)\Delta t/v}) & 0 \\ \frac{1}{2}(1 - e^{(-r/v)\Delta t}) & \frac{1}{2}(1 - e^{(-r/v)\Delta t}) & e^{(-r/v)\Delta t} & 0 & 0 \\ 0 & 0 & 0 & 0 & 1 \\ 0 & 0 & 0 & 0 & 1 \end{vmatrix} \tag{19}$$

In the above matrix, the probabilities located on the diagonal are the probabilities of remaining in the same vessel, those on the vertical columns are the probabilities of entering vessel j and those located on the horizontal rows correspond to the probabilities of leaving vessel j.

Every transition probability can be rewritten making use of dimensionless variables, bearing in mind that according to assumption 4,

$$v = V/4 \tag{20}$$

and defining a recycle ratio

$$R = \frac{r}{Q} \tag{21}$$

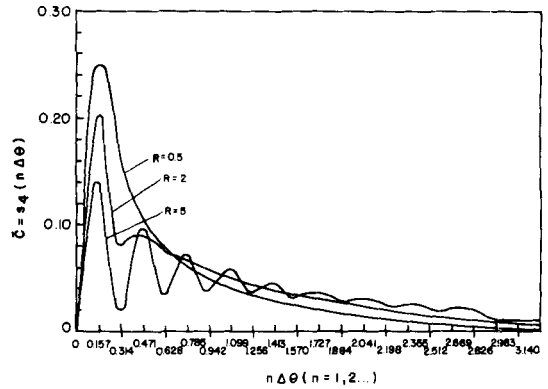

a: Theoretical Response to a Pulse Input for $\Delta\theta = 0.157$ and R = 0.5, 2, 5

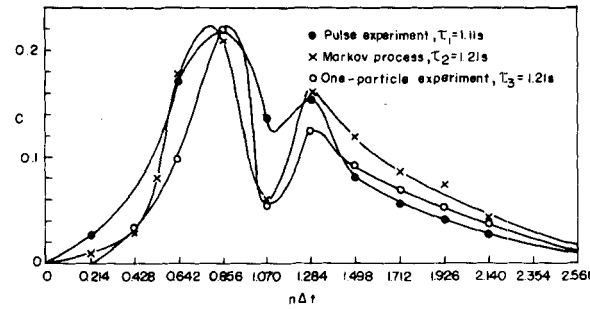

b: Comparison between theoretical and experimental results

Figure 5. Response curves to a pulse input in a two-impinging-streams reactor.

where V is the holdup of the whole reactor and v is the holdup of each vessel i. Also a dimensionless time interval is defined by:

$$\Delta\theta = \Delta t \frac{Q}{V} \tag{22}$$

We also know the initial state probability vector (Figure 4(c)):

$$S(0) = s_1(0), s_2(0), s_3(0), s_4(0), s_5(0) = 0.5, \quad 0.5, \quad 0, \quad 0, \quad 0 \tag{23}$$

since a particle has an equal probability of entering the system at vessel 1 or 2, and probability zero to enter at any other vessel.

General curves of the reactor response to a pulse input, based on the Markov model and obtained by computer simulation, are shown in Figure 5a in terms of $\bar{C} = s_4(n\Delta\theta)$ vs. $n\Delta\theta$ ($n = 1,2,\ldots$). The parameters of the curves are R and $\Delta\theta$. The main features which characterize the curves so obtained are: a) the number of oscillations N_o; and b) the height h of the first response of the system ($n = 1$) to the pulse input. We shall now see how these characteristics can be of help in finding the correct sampling time interval.

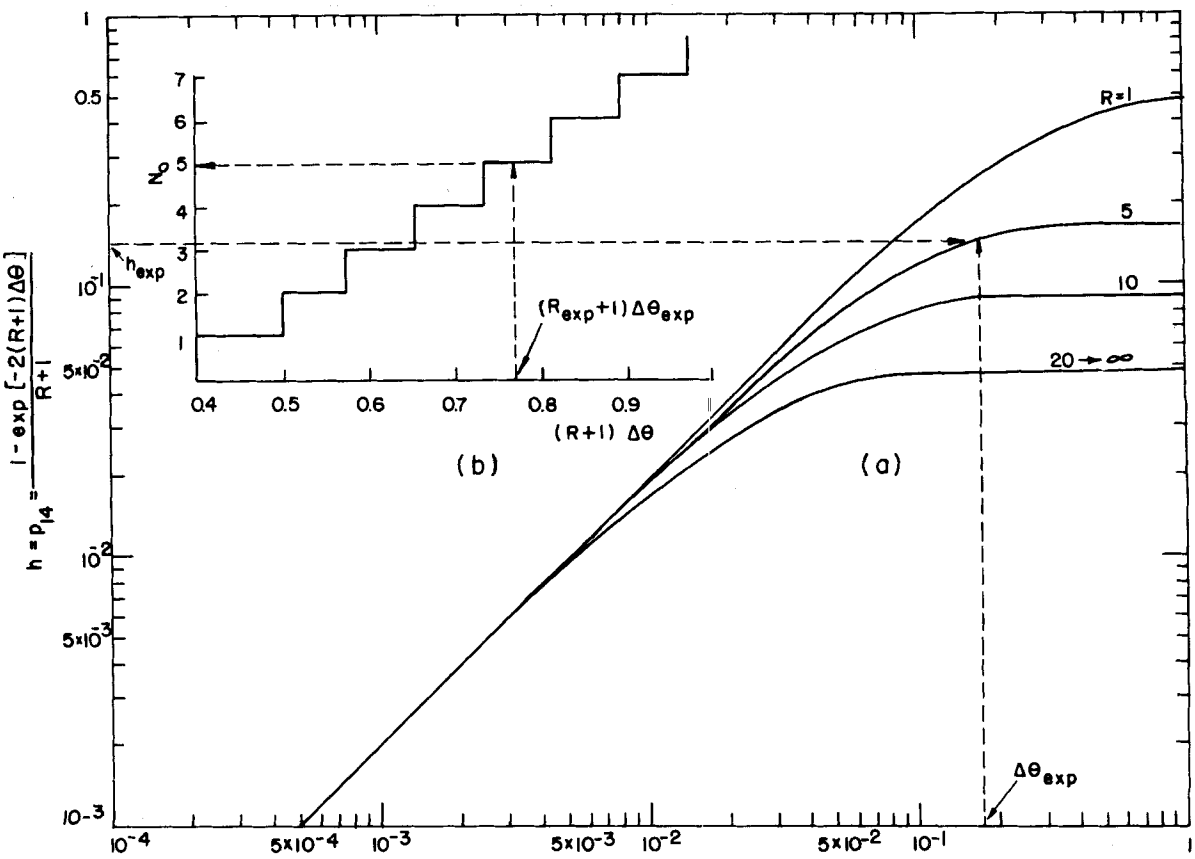

Figure 6. Determination of $\Delta\Theta$: probability of leaving the system in one step vs. dimensionless time interval.

Procedure for Finding Correct $\bar{C}$ Curve

The first response of the system (h) to a pulse input, as calculated from the model, has been plotted in Figure 6(a), as a function of the parameter $\Delta\Theta$ for different values of R. It has also been found that the number of oscillations present in the response curve is a function of the value $(R + 1)\Delta\Theta$ as seen in Figure 6(b). These two plots enable us to find very quickly the shortest sampling interval which gives a reasonably small experimental shift from the true value. The theoretical basis of the procedure will be discussed later, said procedure consisting of the following steps:

1. We chose any angular velocity which is reasonable according to the operating conditions, perform a pulse experiment, draw the resulting response curve, Figure 3(c), and calculate the mean residence time by the following equation (assuming identical values of Δt):

$$\tau = \frac{\int_0^\infty C\,t\,dt}{\int_0^\infty C\,dt} \cong \frac{\sum_{i=1}^{n} C_i t_i \Delta t}{\sum_{i=1}^{n} C_i \Delta t} = \frac{\sum_{i=1}^{n} C_i t_i}{\sum_{i=1}^{n} C_i} \qquad (24)$$

where n is the total number of sections containing tagged particles in our sampling device (Figure 4(d,e)), C_i is the number of tagged particles in section i and $t_i = i\Delta t$.

2. From the knowledge of the angular velocity and τ we know the value of $\Delta\Theta$ and from the experimental curve the value of N_o. With the aid of these two values we read the value of the recycle ratio R, as shown in Figure 6(a).

3. We are now able to read the number of expected oscillations N_o from Figure 6(b).

4. If the value of N_o from the figure is higher than the experimental one, we increase the length of the sampling time interval, else, we decrease it. The reason for decreasing the sampling speed, (and therefore for increasing the sampling interval) is that, when the experimental error is too high, random oscillations appear in the response curve which have no physical reason to be.

5. We repeat this procedure until the expected and experimental values of N_o are equal. Usually, not more than three pulse experiments are needed in this trial and error procedure before the desired value (and accordingly the correct RTD curve) is found. This can be checked by repeating the pulse experiment with the same sampling time interval. Since the experimental error is small, very similar curves must be obtained for two subsequent experiments.

DISCUSSION

We assumed that the stochastic model we presented describes the true behavior of the investigated system closely enough. This hypothesis was tested in a simple way, taking into account the following considerations: in the present case, the Markov model deals with the probability of finding a particle at the reactor exit within a certain interval of time from its entering the reactor. In other words, to prove the validity of the theoretical model. it is necessary to carry out several experiments with a single particle and to see whether, within a certain interval of time from the beginning of the process, the experimental probability is equal to the probability predicted by the model previously established.

This has been done as follows. Operation conditions were chosen at random and a pulse experiment with about 200 tagged particles injected to the main stream of particles was carried out according to the procedure described in the previous section. The experimental RTD curve and the curve predicted by the model, making use of the parameters found from Figure 6 are plotted in Figure 5b. Furthermore, experiments were carried out by throwing just one tagged particle into the main stream of particles and air and recording its exit time. This experiment was repeated a large number of times, until the exit time distribution curve was seen to remain virtually unchanged. The curve for this case is shown in Figure 5b (open circles), together with the aforementioned curves. The prominent fact is the close fit of the curve obtained from single-particle experiments and the theoretical curve obtained from

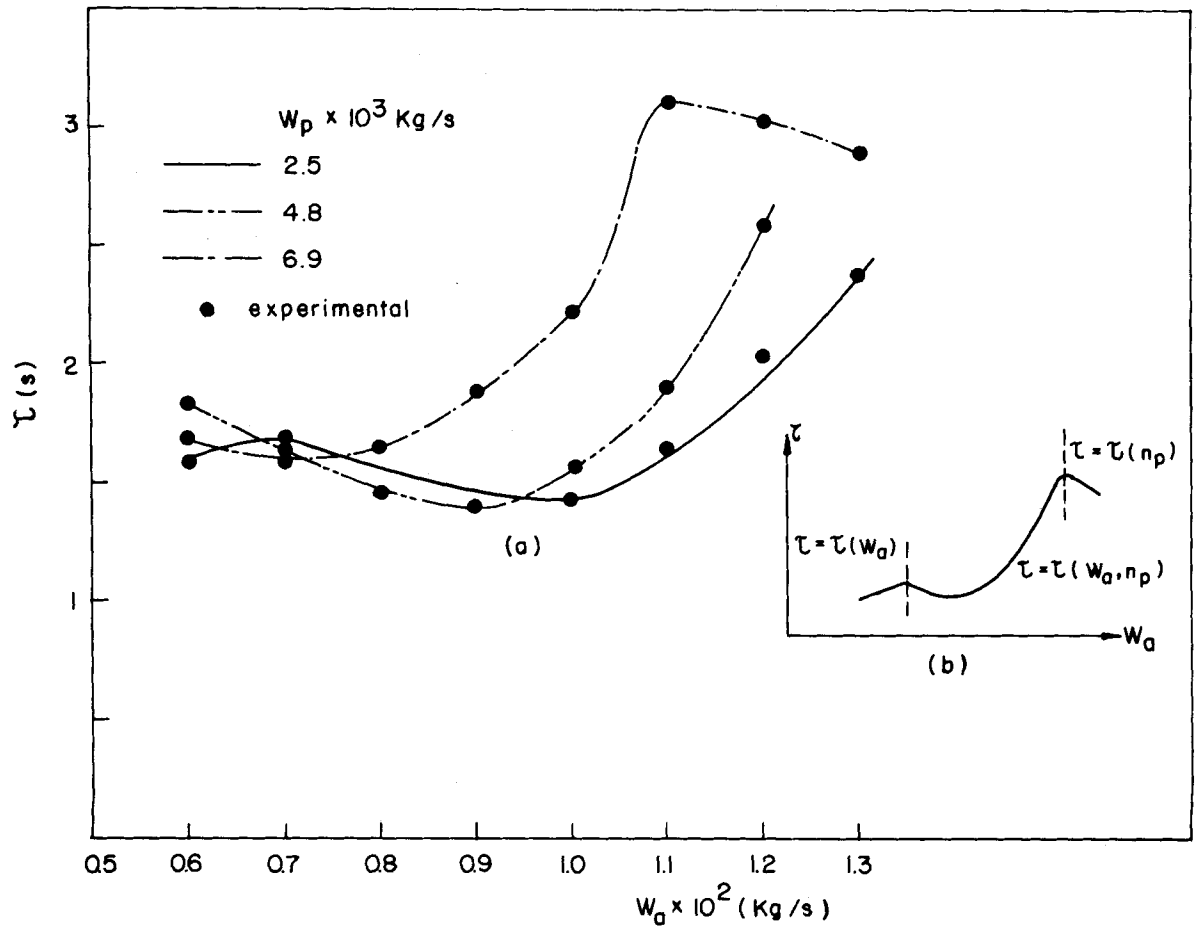

Figure 7. Dependence of the mean residence time on the air flow rate.

parameters fitting on the basis of experiments done with a single pulse containing many particles. The agreement is even better than the agreement between the latter curve and the experimental curve based on a pulse with many tagged particles, as it is seen also from the numerical value of τ. The reason for this behavior is that a pulse experiment with one tagged particle may indeed be considered as a perfect pulse in comparison to a pulse experiment with many particles.

The validity of the Markov model for describing the true $\overline{C}$ curve indicates that, to obtain a reliable curve, the theoretical Δt of the various processes occurring within the reactor as defined in the model, must be equal to the experimental Δt needed to pass one triangular section of the circular plate. Mathematical models of the kind of the stirred tanks in series cannot be of help since their parameters cannot be determined. The parameters for such models can be found by fitting the experimental $\overline{C}$ curve, but there is no way to ascertain whether the curves are correct or not, as it is done in our case.

Oscillatory Behavior

The oscillatory behavior of solid particles at the active volume of the reactor (between points 9 and 11 in Figure 1) plays a major role in its performance and, therefore, deserves detailed consideration.

The harmonic motion of the particles at the circumference of the reactor is possible due to the force acting thereon, known as the Magnus or Segre-Silberberg effect. Said effect causes the particles to move towards the center of the annulus (between points 4 and 5 in Figure 1) thereby partly avoiding direct collision with the walls of the reactor. The existence of this effect and the harmonic motion of the particles around the impingement point have been checked by inspection. However, we felt that this required the following analyses.

1. Qualitative Analysis. A particles mass flow rate has been chosen at random, and the speed of rotation of the device of Figure 4(d,e) has been adjusted at a value for which, for the minimal permissible air flow rate, all the tracer of a pulse experiment was collected in 4–5 sections of the rotating device. The air flow rate has been gradually increased through separate pulse experiments, while leaving the speed of rotation of the device unchanged. It has been noted that, with increasing air flow rate, the number of sections of the rotating device required to collect all the tracer increases. This result is suggestive of an increase of oscillatory motion of the particles within the reactor, with retarded release of the tracer.

2. Quantitative Analysis. Pulse experiments have been carried out for different particles and air flow rates and the dependency of the mean residence time, τ, on the air mass flow rate has been determined. The results for three representative situations are summarized in Figure 7(a). The situation is complex since two maxima and a minimum characterize this dependency. A general curve of such behavior is depicted in Figure 7(b) in which three different zones can be visualized.

1) The first zone in which τ is increased and attains a maximum with increasing air flow rate. In this zone we assume that τ is a function of the air flow rate alone, $\tau = \tau(w_a)$.

2) In the second zone, τ reaches a minimum before starting to grow rapidly towards yet another maximum. It is believed that in this zone two factors influence the value of τ. When we increase the air flow rate, we indeed cause an oscillatory motion of the particles within the reactor, which in turn causes a larger number of particles to be held in the impingement zone. However, the larger the number of particles the greater the probability of collisions with immediate discharge of the colliding particles. Therefore, in the second zone, oscillations and collisions act on the mean residence time in opposite directions and $\tau = \tau(w_a, n_p)$.

3) In the third zone the density of particles is so high that the

mean residence time is decreased by collisions and the oscillatory behavior plays a minor role in determining its magnitude. In this region $\tau = \tau(n_p)$.

In the present experiments, we could not reach conditions at which it was possible to obtain the entire curve as shown in Figure 7(b) for a certain particles mass flow rate. However, the three curves in Figure 7(a) lead to the conclusion that a general behavior would be such as depicted in Figure 7(b).

Pumping Energy

Table 1 indicates that the maximal pumping work per kg of solids transported by air through our reactor is 0.47 kJ/kg. An evaluation of this figure may be done by considering two examples taken from Romankov and Rashkovskaya (1964). The first one deals with drying of peat fuel particles ($D_p = 0.5 \times 10^{-3} - 3 \times 10^{-3}$ m) in a fluidized bed. For $w_a = 4.55$ kg/s and $w_p = 0.69$ kg/s it is obtained that $\Delta P = 2{,}309$ Pa. These data yield a specific pumping energy of 12.2 kJ/kg peat. The other example indicates that drying of a plumbum dye paste in a fluidized bed is carried out so that $w_a = 0.091$ kg/s; $w_p = 0.014$ kg/s, $\Delta P = 4{,}900$ Pa which yields a specific pumping energy of 16.9 kJ/kg.

The above figures are 26–36 times higher than the maximal value of the specific pumping energy needed in our reactor. This difference indicates the high efficiency of the new reactor with respect to pumping energy requirements. In a fluidized bed a considerable part of the energy is needed to maintain the particles in a fluidized state as well as to introduce the air through the gas distributor or constriction plate. It should be emphasized that the above figures were confirmed by Tamir and Luzzatto (to appear) both in a fluidized bed or a spouted bed. It may be concluded that the two-impinging-streams reactor consumes pumping energy less.

NOTATION

C = concentration, counts or number of particles collected per unit time
$\overline{C}$ = mean concentration at a certain time, Eq. 8
D = diameter of inlet tubes to the reactor (2 in Figure 1), m
Eu = Euler number ($\Delta P/\rho_a U_a^2$)
$\overline{Eu}$ = ratio between Euler numbers of the large-scale equipment and laboratory apparatus
h = height of first response to a pulse input
$\overline{L}$ = ratio between all length dimensions of the large-scale equipment and the laboratory apparatus
m = number of repetitive experiments
n = number of transitions in the Markov process
n_p = number of particles
N = number of possible states for transition of the system in the Markov process
N_o = number of oscillations in the response to a pulse input
p_{ij} = transition probability
P = transition matrix
Q = particles input stream flow rate in the model, kg/s
r = recycle stream flow rate, kg/s
R = recycle ratio (r/Q)
Re = Reynolds number (DU_a/ν_a) based on mean velocity at inlet pipes (2, in Figure 1)
$\overline{Re}$ = ratio between Reynolds numbers of the large-scale equipment and the laboratory apparatus
RTD = residence time distribution
s_i = state probability
S = state probability vector
t = time, s
U = velocity, m/s
v = holdup of a vessel in the model, kg
V = holdup of the reactor, kg
w = mass flow rate, kg/s

Greek Letters

ΔP = pressure drop, Pa
μ = the ratio, w_p/w_a
ρ = density, kg/m^3
ν = kinematic viscosity, m^2/s
η = the ratio, Eu_p/Eu_a
Θ = dimensionless time (t/τ)
τ = mean residence time, s, Eq. 24

Subscripts

a = air
exp = experimental
ij = states in the model
p = particles

LITERATURE CITED

Elperin, I., and A. Tamir, "Method and Reactor for Effecting Interface Reactions," Israeli Patent Application No. 66162 (1982).

Elperin, I., K. Luzzatto, and A. Tamir, "A New Two-Impinging-Streams Heterogeneous Reactor," Canadian Chem. Eng. Conf., Vancouver, British Columbia (Oct. 3–6, 1982).

Gibilaro, L. G., W. H. Kropholler, and D. J. Spikius, "Solution of A Mixing Model Due to Van de Vusse by a Simple Probability Method," *Chem. Eng. Sci.*, **22**, 517 (1967).

Gukhman, A. A., *Introduction to Similitude Theory*, "Higher School," Moskow (1973).

Howard, R. A., *Dynamic Programming and Markov Processes*, Wiley, New York (1960).

Kunii, D., and O. Levenspiel, *Fluidization Engineering*, Wiley, New York (1960).

Leva, M., *Fluidization*, McGraw-Hill, New York (1959).

Mikheev, M. A., and E. M. Mikheeva, *Fundamentals of Heat Transfer*, Moskow, "Energy" (1977).

Romankov, P. G., and N. B. Rashkovskaya, "Drying in Fluidized Bed (Theory, Apparatus, Design)," *Chemistry*, Moskow-Leningrad (1964).

Tamir, A., I. Elperin, and K. Luzzatto, "Drying in a Two-Impinging Streams Heterogeneous Reactor," *Chem. Eng. Sci.* **39**, 1 (1984).

Tamir, A., and K. Luzzatto, "Solid-Solid Gas-Gas Mixing Properties of a New Two-Impinging-Streams Mixer, *AIChE J.*, (to appear).

Van de Vusse, J. G., "A New Model for the Stirred Tank Reactor," *Chem. Eng. Sci.*, **17**, 507 (1962).

Manuscript received January 12, 1983; revision received and accepted July 14, 1983.